Diffraction line-profile shape by synchrotron and laboratory x-ray sources[*]

Davor Balzar[1,3], Peter W. Stephens[2], and Hassel Ledbetter[1]

[1] Materials Science and Engineering Laboratory, National Institute of Standards and Technology, 325 Broadway, Boulder, CO 80303
[2] National Synchrotron Light Source, Brookhaven National Laboratory, Upton, NY 11973
and
Physics Department, State University of New York, Stony Brook, NY 11794
[3] On leave from X-ray Laboratory, Division of Materials Research and Electronics, Physics Department, Ruđer Bošković Institute, P.O. Box 1016, 10001 Zagreb, Croatia

ABSTRACT

We compared diffraction-line profiles obtained at the X3B1 NSLS powder-diffraction beamline and with a standard $CuK\alpha_{1,2}$ sealed source. An NIST SRM LaB_6 was used as the standard material to study the effects of different instrumental parameters. We show that the equatorial-slit width has a major influence not only on vertical (equatorial) divergence but also on the character of diffraction-line profiles at high angles. A theoretical expression for peak width based on the Gauss approximation for transmission functions of all optical elements fails at high angles probably because of the inadequacy of the Gauss approximation for the shape of the monochromator Bragg reflection. The minimum number of parameters that have to be refined in a Rietveld code for a standard specimen is discussed.

INTRODUCTION

Precise knowledge of diffraction line-profile shape is of utmost importance in x-ray powder diffraction, especially in line-broadening analysis, Rietveld refinement, and other whole-powder-pattern-fitting programs. In this regard, laboratory x-ray sources were researched extensively in the past, but synchrotron radiation remains inadequately characterized, despite its increasingly frequent recent use. Most of the line-profile models rely on a milestone study of Caglioti, Paoletti, and Ricci[1] that was developed for neutron diffraction and later adapted in the synchrotron case.[2] Basic studies of synchrotron powder diffraction were undertaken by Cox et al.[3], who also gave a comprehensive review[4] of the field.

Synchrotron radiation is inherently advantageous to laboratory sources for line-broadening studies for many reasons: naturally high beam collimation provides a superior resolution, the wavelength of a monochromatic beam can be easily tuned, and line shape is generally simpler and controlled to our preference. Most important, however, is the high resolution, that is, the narrow instrumental line profile implies a high sensitivity to the small physical broadening.

---

[*] Noncopyrightable U.S. government contribution.

EXPERIMENTAL SETUP

For the laboratory measurements, we used a horizontal goniometer in divergent Bragg-Brentano flat-plate geometry with both incident and diffracted Soller slits to minimize axial beam divergence, 2 mm divergent and 0.2 mm receiving slits. Cu $K\alpha_{1,2}$ radiation was scanned with a cooled germanium solid-state detector. Synchrotron-radiation measurements were performed on the X3B1 beamline at the National Synchrotron Light Source (NSLS), Brookhaven National Laboratory. The triple-axis parallel geometry included Si channel-111-cut monochromator, flat specimen, Ge 111-cut analyzer crystal, and proportional detector (Figure 1). Typical NIST SRM LaB_6 diffraction line-profiles are presented in Figure 2. At this diffraction angle, synchrotron radiation gives four times smaller line width and 2.5 times larger peak-to-background ratio, despite twice as large a background count. Both line profiles are closely approximated with the Voigt function or its pseudo-Voigt and Pearson VII approximations.[4] However, it is still a matter of debate[5] why the line profiles tend to be almost pure Lorentz functions at high angles, the same effect that is observed for laboratory sources. Therefore, it is desirable to study the overall effect of geometrical aberrations on the diffraction-line shape.
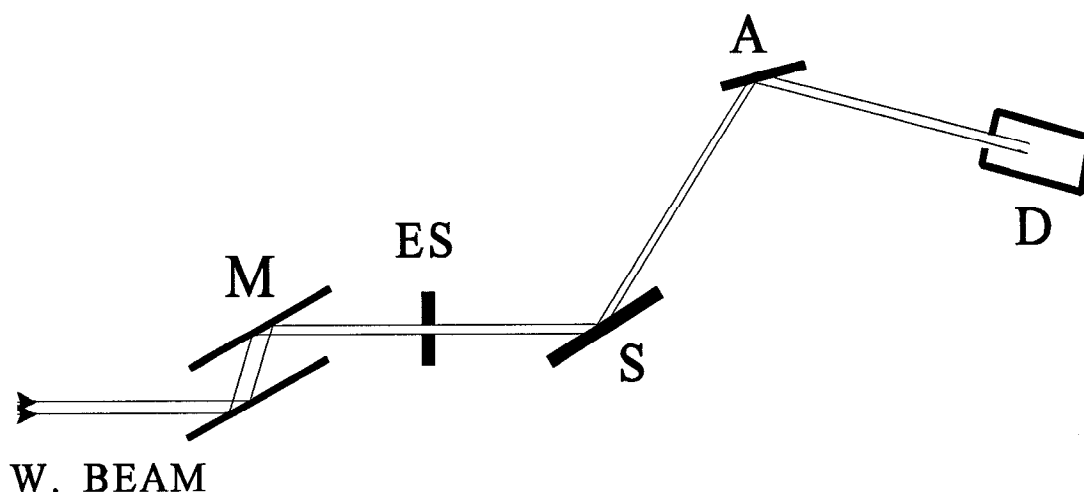

Figure 1 Schematic view of X3B1 NSLS beamline in the (vertical) equatorial plane. M: monochromator crystal; ES: equatorial slit; S: specimen; A: analyzer crystal; D: detector.
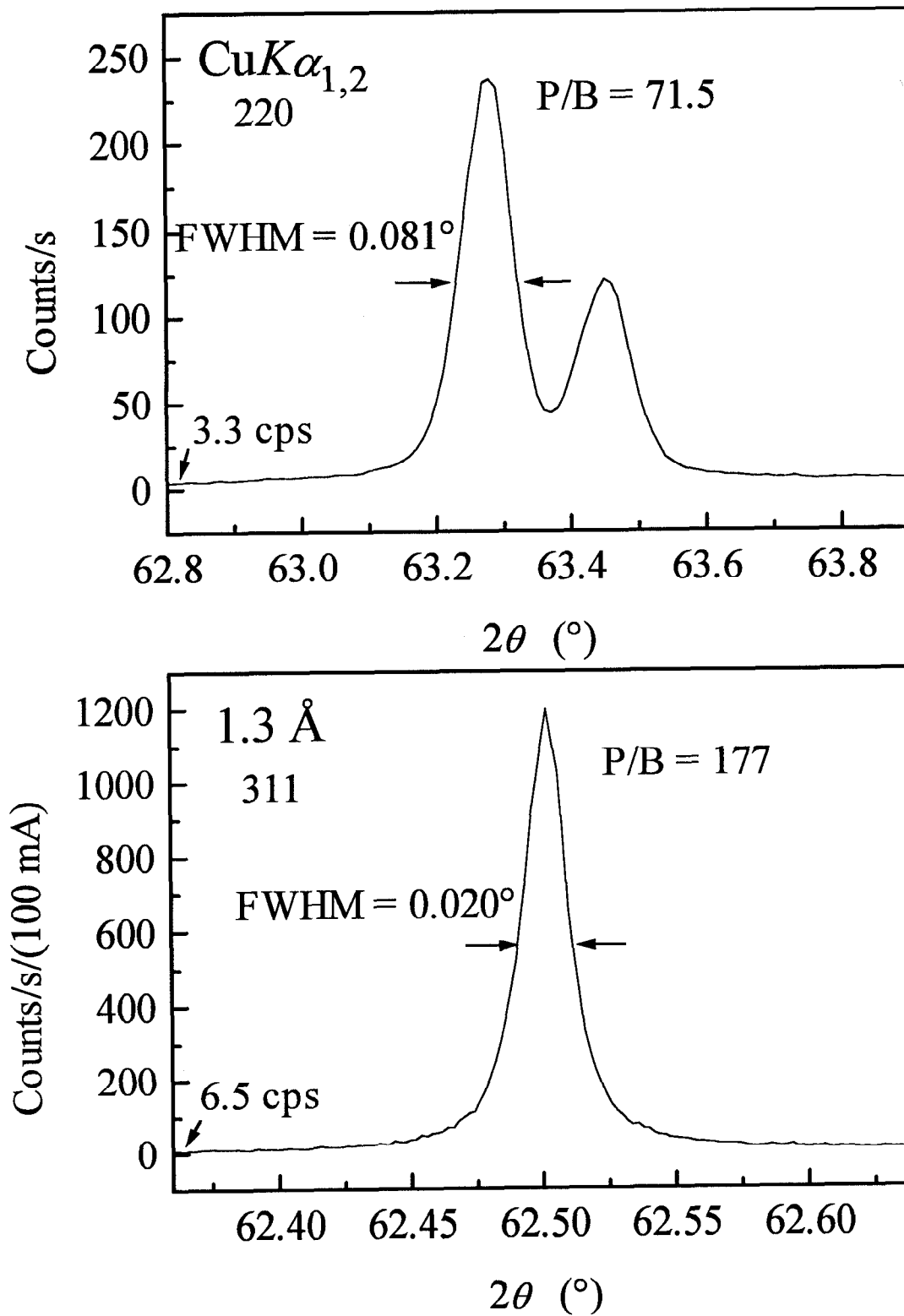
Figure 2 Diffraction-line profiles of NIST SRM LaB_6 obtained at laboratory and synchrotron (NSLS) x-ray sources. P/B denotes the peak-to-background ratio.

SYNCHROTRON DIFFRACTION-LINE SHAPE

The main equatorial instrumental factors affecting the diffraction-line profile and/or position are the following:

(i) Source height (vertical angular distribution of the polychromatic beam) is approximated with the Gauss function at the bending magnet. It depends on the storage-ring electron (positron) relativistic factor γ, the photon energy ϵ, and the critical photon energy ϵ_c (5.04 keV at NSLS):

$$g_S(z) = \exp(-4\ln 2\, z^2 / \mathrm{FWHM}_\phi^2), \tag{1}$$

where the vertical (equatorial, for it is in the scattering plane) divergence is

$$\mathrm{FWHM}_\phi = \frac{1.331}{\gamma(\epsilon_c/\epsilon)^{0.425}}; \quad \gamma = [1-(v/c)^2]^{-1/2} = E/(m_0 c^2). \tag{2}$$

Here, v, E, and m_0 are the electron (positron) speed, energy, and rest mass, respectively, and c is the speed of light.

(ii) Equatorial slit width:

$$g_{ES}(z) = \begin{cases} 1 & |z| \le a/2 \\ 0 & |z| > a/2 \end{cases} \tag{3}$$

(iii) Normalized Darwin Bragg-reflection shape[6] of the monochromator and analyzer (perfect) crystals (rocking curve):

$$g_{M,A}(z) = s^2 / [z \pm (z^2 - s^2)^{1/2}]^2 \tag{4}$$

Here, s defines the region for a perfect reflection (without absorption) from a crystal.

(iv) Specimen effects that cause important aberrations in laboratory divergent geometry, such as transparency, flat surface, and its missetting, are negligible in synchrotron parallel geometry with the analyzer crystal.

The most important axial aberration is a divergence, which sometimes causes severe asymmetry at low angles. The effect on powder line shapes was considered by van Laar and Yelon[7] and recently applied to high-resolution synchrotron diffractometers by Finger, Cox, and Jephcoat.[8]

The total diffraction-line profile results from a convolution of all the contributions, which has to be accomplished numerically. However, for most purposes, a simple estimation of line widths as a function of diffraction angle may suffice. Wavelength dispersion follows from the Bragg law:

$$\Delta\lambda/\lambda = (\omega_M^2 + \omega_A^2 + \mathrm{FWHM}_\phi^2)^{1/2}\cot\theta. \tag{5}$$

Here, the shape of perfect Bragg reflection is approximated with the Gauss function. ω_M and ω_A designate monochromator and analyzer-crystal Darwin widths. They depend on the structure factor, polarization, absorption, and temperature (see for instance Warren[6]).

To recognize the relative importance of various contributions, we estimate the angular resolution at the X3B1 NSLS beamline with 8 keV photon energy, that is, the approximate Cu Kα wavelength:
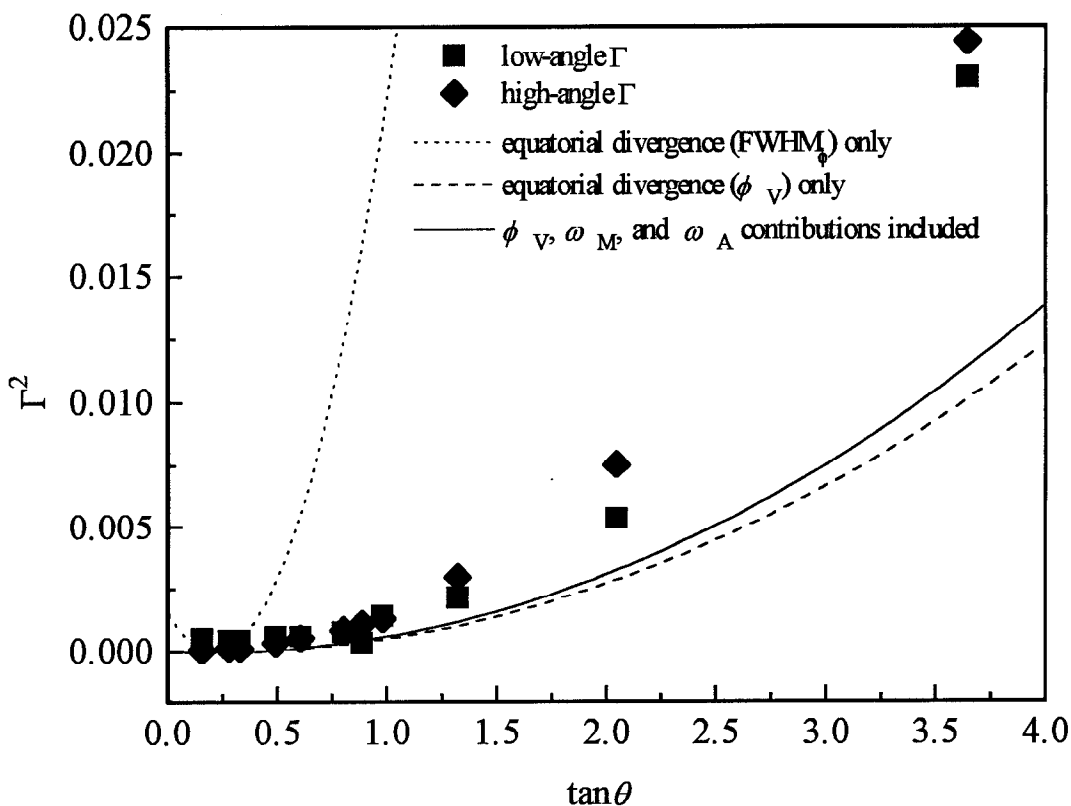
Figure 3 FWHM Γ of split-Pearson VII fits to the line profiles of LaB_6 and different broadening models presented with lines.

$$FWHM_\phi (2.5 \text{ GeV}, 8 \text{ keV}) = 0.0190° \, ;$$
$$\omega_M(111 \text{ Si}, 8 \text{ keV}) = 0.0021° \, ; \quad \omega_A(111 \text{ Ge}, 8 \text{ keV}) = 0.0045° \, . \tag{6}$$

It seems that the Darwin widths of both analyzer and monochromator crystals make a minor contribution and can be neglected in the first approximation. However, this large a divergence would yield very poor resolution (see Figure 3) and it must be controlled by the narrow equatorial slit in front of the specimen. The $FWHM_\phi$ yields the height of the beam at the slit position of about 4.5 mm for the X3B1 beamline (ring-slit distance is 13.7 m). Usually, at least three times narrower slit has to be used to improve the resolution. For instance, we collected the LaB_6 data at 1.30049(3) Å with 0.75 mm equatorial-slit width (Figure 3). Line profiles were fitted with a split-Pearson VII function to model the peak asymmetry effects. The main peak-width contributions are now

$$\phi_V = 0.0031° \, ;$$
$$\omega_M(111 \text{ Si}, 9.54 \text{ keV}) = 0.0015° \, ; \quad \omega_A(111 \text{ Ge}, 9.54 \text{ keV}) = 0.0032° \, . \tag{7}$$
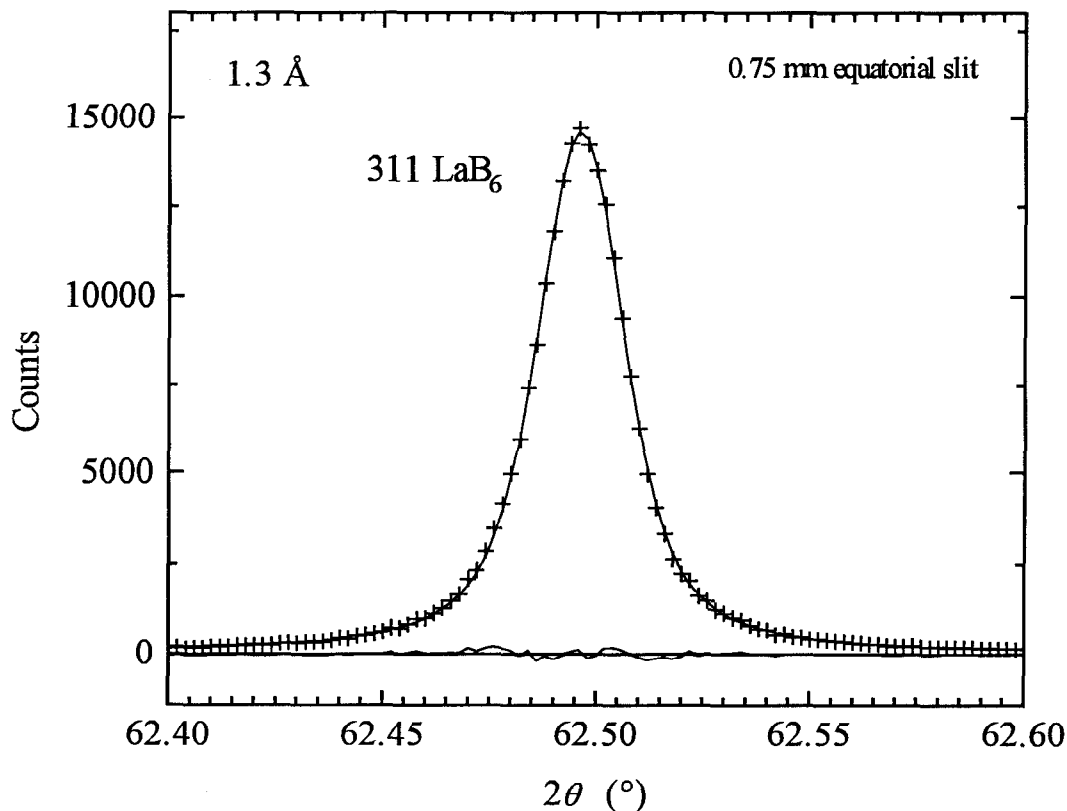
Figure 4 Voigt-function fit (full line) to the 311 LaB$_6$ profile (crosses). The difference pattern is given below.

Here, the vertical divergence ϕ_V is defined by the equatorial slit. Certainly, the monochromator and analyzer Darwin widths become significant. To calculate the FWHM, we use the expression of Sabine:[2]

$$
\begin{aligned}
\Gamma^2 &= \phi_V^2 (2\tan\theta/\tan\theta_M - \tan\theta_A/\tan\theta_M - 1)^2 \\
&+ \omega_M^2 (2\tan\theta/\tan\theta_M - \tan\theta_A/\tan\theta_M)^2 + \omega_A^2 \\
&+ (w_{ES}^2 + w_{RS}^2)/(12 D_{SR}^2).
\end{aligned}
\tag{8}
$$

Here, we add the influence of specimen size (which approximately equals the equatorial-slit width w_{ES}) and receiving-slit width w_{RS}, where D_{SR} is the distance from specimen to receiving slit. This term can be neglected when the analyzer crystal is used. Note that the slit-width contribution to the variance W is weighted by the factor 1/12 (compare to Wilson[9]):
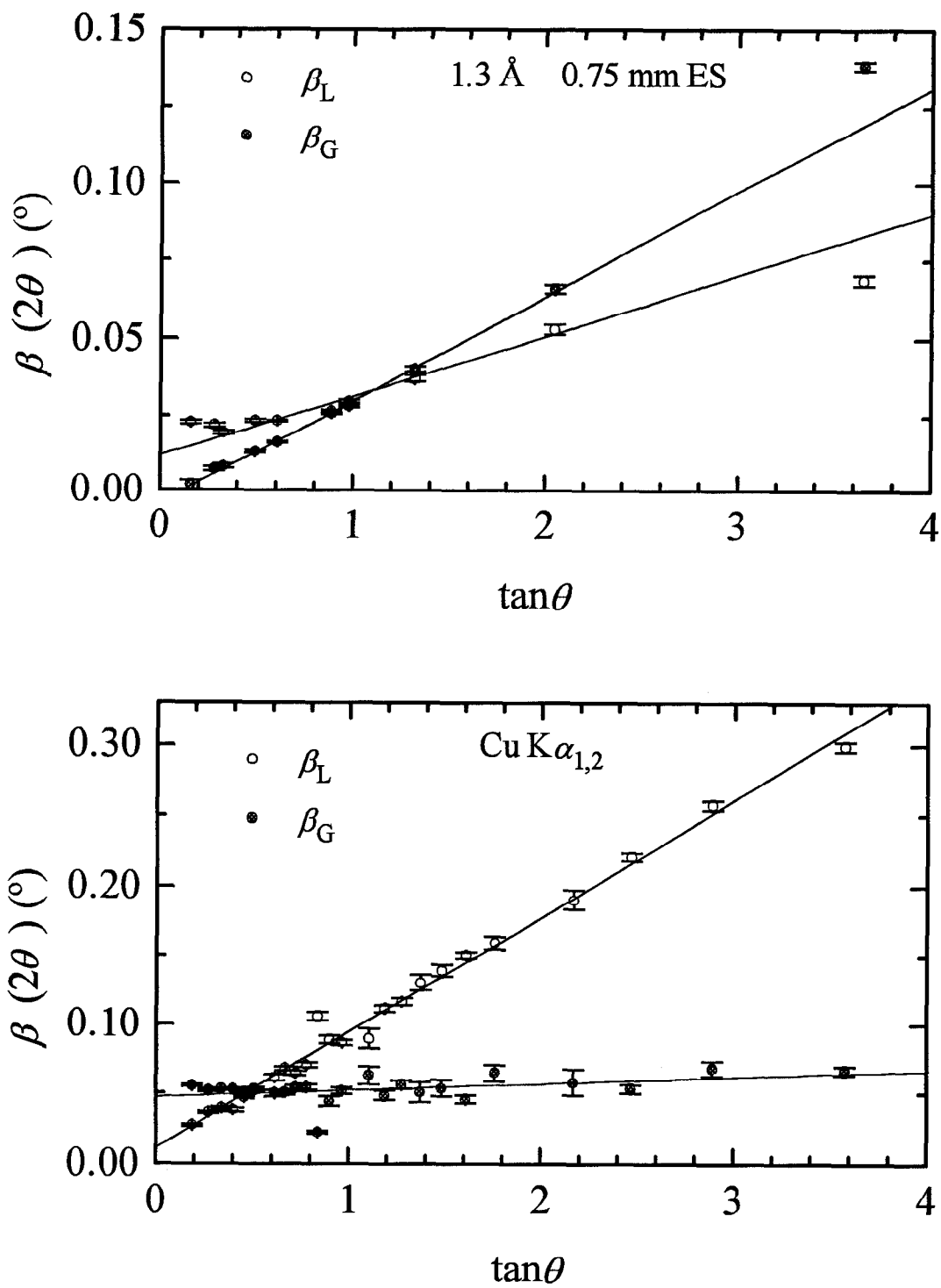
Figure 5 Parameters of Voigt-function fits to LaB_6 peaks using synchrotron (upper) and laboratory (bottom) source. Linear regression curves not fitted through the first two lines because of asymmetry.
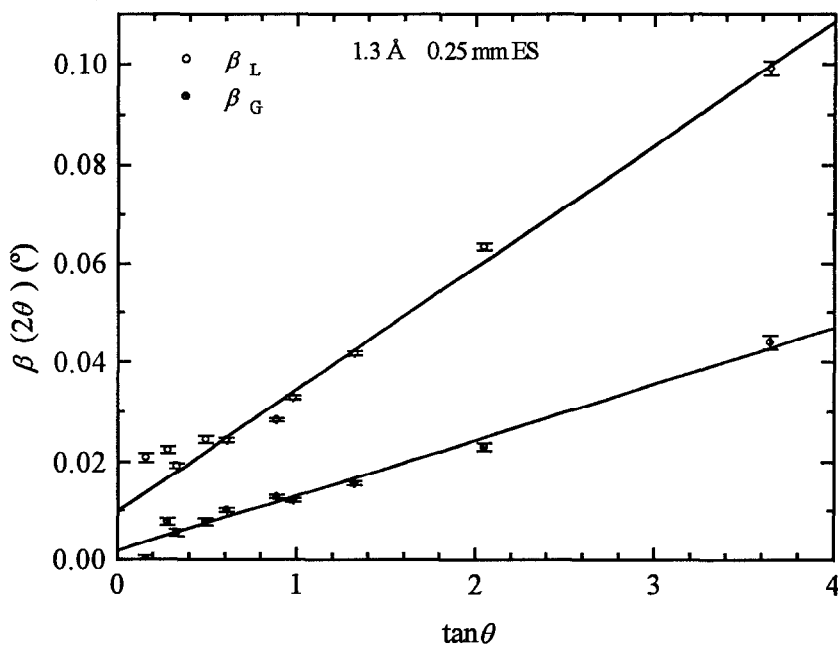
Figure 6 The parameters of Voigt-function fits to line profiles of LaB_6 using narrower entrance slit.
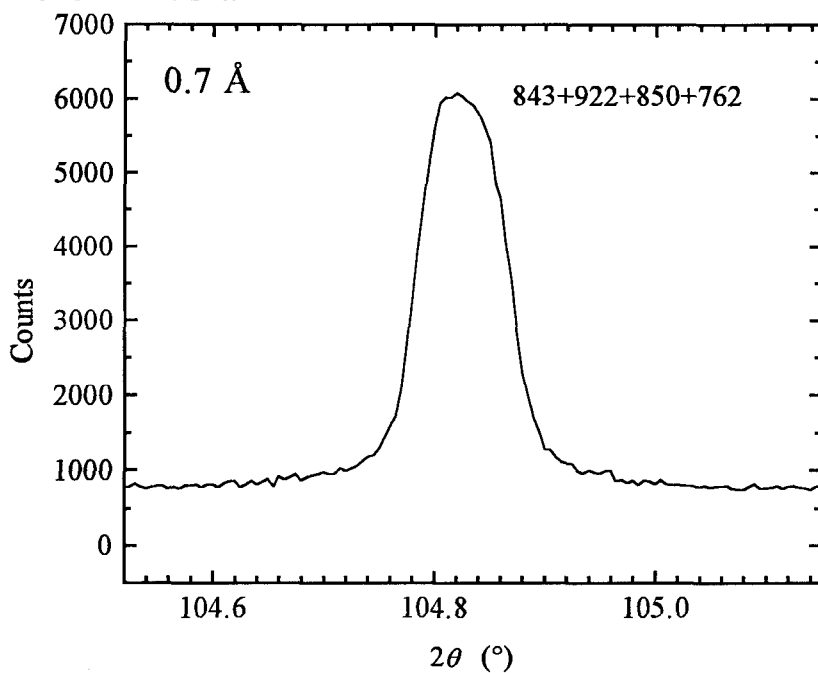

Figure 7 LaB_6 line profile recorded with the 1.5 mm wide equatorial slit.

$$W = \frac{\displaystyle\int_{-1/2w/D}^{1/2w/D} (2\epsilon - \langle 2\epsilon \rangle)^2 \, d(2\epsilon)}{\displaystyle\int_{-1/2w/D}^{1/2w/D} d(2\epsilon)} = \frac{1}{12}\left(\frac{w}{D}\right)^2. \tag{9}$$

The peak centroid is not affected by slits ($\langle 2\epsilon \rangle = 0$). Here, we neglect a possible variation of intensity across the slit width.

In Figure 3 we plot three curves: the equatorial divergence term given by $FWHM_\phi$, the first term of (8), and the first three terms of (8). The monochromator-related wavelength (energy) dispersion has a major influence at high diffraction angles, but the analyzer as well as slit contributions are quite small, except at low angles. The fit is satisfactory up to about 80° in 2θ. There are two possible reasons why (8) is not a good approximation at high angles: residual physical broadening of LaB_6 and/or the inadequacy of (8), because it assumes that the transmission functions of all optical elements that contribute to broadening follow a Gauss distribution. That may be a fair approximation in the neutron-diffraction case, but certainly not for synchrotron-radiation diffraction, where profiles have a significant Lorentz contribution. To further examine this matter, we fit the same peaks with an exact Voigt function so the Lorentz and Gauss parts are separated. The typical fit is presented in Figure 4. Figure 5 compares measurements of an NIST SRM LaB_6, obtained both with synchrotron and laboratory sources. Very different behavior of the Gauss part suggests that potential physical broadening of NIST SRM LaB_6 cannot be significant and that the different behavior stems from the instrumental parameters. For laboratory sources, the Gauss part is given mainly by the source and receiving-slit size and is approximately constant in 2θ, and the Lorentz part is dominated by wavelength dispersion

$$\beta_L = 2\Delta\lambda/\lambda \tan\theta, \tag{10}$$

as pointed out by Klug and Alexander[10] and Cox.[4]

Figure 3 shows that the major influence on peak width comes from the equatorial divergence of the beam and from wavelength dispersion at the monochromator. Although the equatorial-beam distribution (1) may have a substantial Lorentz contribution, which would cause discrepancy at high angles, the latter effect is dominant at higher angles for this monochromator (channel-cut) configuration. It is likely that long tails of the shape of monochromator Bragg reflection (see (4)) contribute substantially to the peak width and are visible as a Lorentz part of fitting a Voigt or a like function. This is confirmed by the measurements with narrower equatorial slit (0.25 mm), presented in Figure 6. The striking difference from measurements with 0.75 mm slit (Figure 5) is a dominant Lorentz character of the profiles at high angles. Therefore, a wider equatorial slit has an effect of cutting off the long tails characteristic of the reflection from the monochromator. This effect may be more significant in constant-wavelength neutron diffraction, where wider slits must be used because of generally poor beam intensities, which results in predominantly Gaussian peaks.

How slits can affect the line profiles is illustrated in Figure 7. The measurement of the LaB_6 reflection was made with 1.5 mm wide equatorial slit. The peak has the appearance of a "super-Gaussian" because the source height (1) is modulated by the slit function (3). The resulting profile is a convolution:

$$g_S * g_{ES} \equiv \int_{-a/2}^{a/2} \exp[-b^2(x-z)^2]\,dz$$

$$= \frac{\sqrt{\pi}}{2b}\left[\mathrm{erf}\left(b\frac{a}{2}-bx\right)+\mathrm{erf}\left(b\frac{a}{2}+bx\right)\right] \tag{11}$$

where

$$b^2 = \frac{4\ln 2}{\mathrm{FWHM}_\phi^2}. \tag{12}$$

Figure 8 presents peak profiles obtained for different ratios of slit width to vertical divergence (FWHM_ϕ), compared with the unmodified Gauss function. If slit width a is smaller than the FWHM_ϕ, the profile stays approximately Gaussian, but there is a loss of intensity. If slit width is increased substantially over the FWHM_ϕ, the "super-Gaussian" shape is obtained. However, there is an advantage in substantial increase of integrated intensity that may outweigh the drawbacks. Moreover, if the specimen shows even a small amount of physical line broadening, the "super-Gaussian" line shape will not be obvious because the physically broadened line profile will smear it out.
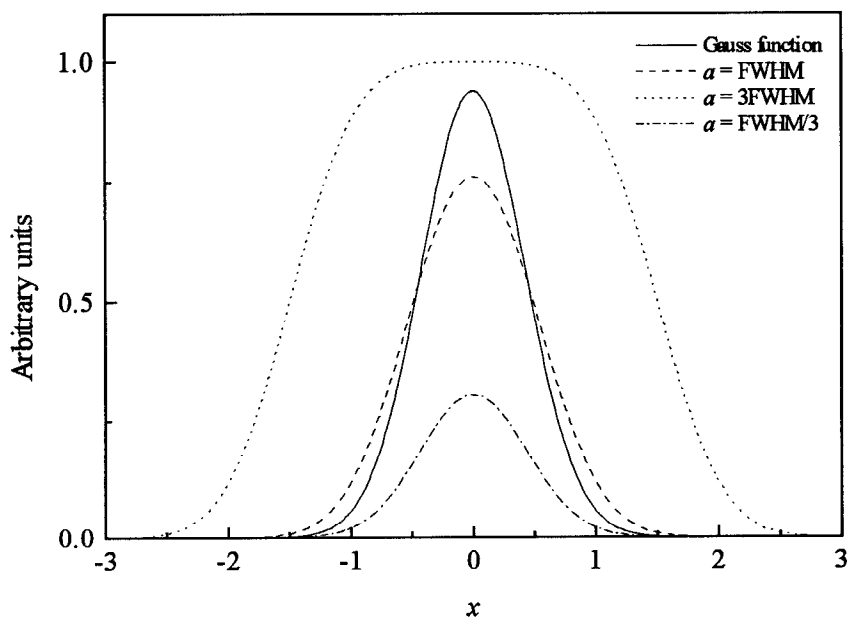

Figure 8 Convolutions of slit function of width a and Gauss function of width measure FWHM for different ratios of a/FWHM.

MODELING OF LINE BROADENING IN RIETVELD REFINEMENT

Most major Rietveld-refinement programs adopt a modified Thompson-Cox-Hastings[11] pseudo-Voigt function to model the symmetrical part of line widths:

$$\Gamma_L = X/\cos\theta + Y\tan\theta + Z;$$ (13)

$$\Gamma_G^2 = P/\cos^2\theta + U\tan^2\theta + V\tan\theta + W.$$ (14)

Figure 5 indicates that, in the case of standard specimen, it is sufficient to vary Y and W coefficients for laboratory sources, but Y, W, Z, and U for synchrotron radiation. The parameter V seems to have no physical merit in either case if Γ_L is being refined.

CONCLUSIONS

Synchrotron radiation is undoubtedly superior to laboratory x-ray sources for diffraction purposes. However, generally a larger number of optical elements is involved in diffraction, which gives more flexibility but also possesses a challenge to the user. Some of the important things to consider are the following:

(i) For usual operating conditions, the contribution of monochromator Darwin width should not be neglected, especially at high angles.

(ii) The total instrumental function (assumed to be represented closely with the measured LaB_6 line profiles) contains the significant Lorentz contribution, which is incompatible with the presumption that all transmission functions are approximately Gaussian.

(iii) The most likely reason why (8) does not describe line broadening at high angles satisfactorily is because the monochromator perfect-Bragg reflection cannot be approximated with a Gauss function.

(iv) Rietveld refinement of a standard specimen requires twice as many profile parameters to vary in the case of synchrotron-radiation data over the laboratory-source measurements.

ACKNOWLEDGMENTS

LITERATURE
1. G. Caglioti, A. Paoletti, and F. P. Ricci, *Nucl. Instrum.* **3** (1958) 223.
2. T. M. Sabine, *J. Appl. Crystallogr.* **20** (1987) 23.
3. D. E. Cox, J. B. Hastings, W. Thomlinson, and C. T. Prewitt, *Nucl. Instrum. Methods* **208** (1983) 573.
4. D. E. Cox, in *Handbook on Synchrotron Radiation*, V. 3, Edited by G. S. Brown and D. E. Moncton, North-Holland, New York, 1991, p. 155.

5. J. I. Langford, R. J. Cernik, and D. Louër, *J. Appl. Crystallogr.* **24** (1991) 913.

6. B. E. Warren, *X-ray Diffraction*, Dover Publications, New York, 1990, p. 324.

7. B. van Laar and W. B. Yelon, *J. Appl. Crystallogr.* **17** (1984) 47.

8. L. W. Finger, D. E. Cox, and A. P. Jephcoat, *J. Appl. Crystallogr.* **27** (1994) 892.

9. A. J. C. Wilson, *Mathematical Theory of X-ray Powder Diffractometry*, Gordon and Breach, Eindhoven, The Netherlands, 1963, p. 15.

10. H. P. Klug and L. E. Alexander, *X-ray Diffraction Procedures*, John Wiley, New York, 1974, p. 290.

11. P. Thompson, D. E. Cox, and J. B. Hastings, *J. Appl. Crystallogr.* **20** (1987) 79.